Pd Nanosheets

DOI: 10.1002/ange.201303772

Shape-Controlled Synthesis of Surface-Clean Ultrathin Palladium Nanosheets by Simply Mixing a Dinuclear Pd^{I} Carbonyl Chloride Complex with H_2O**

*Huan Li, Guangxu Chen, Huayan Yang, Xingli Wang, Jinghong Liang, Pengxin Liu, Mei Chen, and Nanfeng Zheng**

During the past decades, shape control of noble metal (NM) nanocrystals has been extensively demonstrated as an effective means to tailor their properties for a wide range of applications such as catalysis, optics, spectroscopy, biological labeling, and photothermal therapy.[1–9] A number of synthetic strategies including photochemical,[10] electrochemical,[11] and templating methods[9,12] have been developed to achieve shape control of NM nanocrystals. Wet-chemical synthesis of NM nanocrystals with well-defined shape usually requires strict control over the kinetics and thermodynamics of the systems.[2,3,13] Therefore, typical shape-controlled syntheses of NM nanocrystals involve the use of additives, such as surfactants, polymer capping agents, small adsorbates, and even biomolecules.[13–20] Although much effort has been devoted to investigating the relationship between the additives and the shape of the obtained NM nanocrystals, it is still a great challenge to address how the additives control the shape of NM nanocrystals at the molecular level.

To gain a better understanding of how the shape control of NM nanocrystals is achieved chemically, our group has recently focused on the use of small strong adsorbates (e.g., CO, amines) for the shape control of Pt and Pd nanocrystals.[13,21–28] For example, CO molecules behave differently in the controlled synthesis of Pd and Pt nanostructures. CO prefers to adsorb on the Pd{111} surface to facilitate the growth of ultrathin Pd nanosheets and tetrapod/tetrahedral nanocrystals having {111} as the main exposure surface.[21,26] But for Pt, the preferential adsorption of CO on Pt{100} induces the formation of Pt nanocubes.[23,25] However, together with small adsorbates, these reactions typically involved the use of weakly binding polymeric capping agents (e.g., polyvinylpyrrolidone (PVP)). The presence of polymeric capping agents in the systems would likely raise the following two issues: 1) The surface of the as-prepared NM nanocrystals is coated by polymeric capping agents. Since the catalytically active sites on the NM nanocrystals would be blocked more or less by the capping agents, their influence on the catalytic performance of NM nanocrystals should not be simply ignored. 2) The co-presence of small adsorbates and polymeric capping agents makes it impossible to discuss how the shape control of NM nanocrystals is achieved without considering the role of polymeric capping agents.

We demonstrate here a facile shape-controlled synthesis of ultrathin Pd nanosheets by simply mixing a Pd carbonyl complex, $[Pd_2(\mu\text{-}CO)_2Cl_4]^{2-}$, with H_2O in the absence of any organic capping agents. This Pd carbonyl complex bearing two bridging CO ligands belongs to a very large family of carbonyl complexes of noble metals.[29,30] The first dipalladium(I) carbonyl complex, $[Pd_2(\mu\text{-}CO)_2Cl_4]^{2-}$, was discovered in 1942,[31] followed by the spectroscopic and X-ray crystallography study to confirm its structure.[32,33] Until now, most studies have focused on its structure and reactivity;[30] the possibility of fabricating Pd nanostructures with well-defined shape from this kind of complex has not been attempted. In this work, we have prepared $[Pd_2(\mu\text{-}CO)_2Cl_4]^{2-}$ by treating $[H_2PdCl_4]$ in CO atmosphere, and characterized it by X-ray single-crystal analysis and X-ray absorption fine structure (XAFS) spectroscopy. From the ^{13}C isotopic studies, we found that $[Pd_2(\mu\text{-}CO)_2Cl_4]^{2-}$ reacted with H_2O to yield ultrathin Pd nanosheets while releasing CO_2. In the absence of organic capping agents, the as-prepared Pd nanosheets have clean Pd{111} as their main exposure surfaces, which provides a great opportunity to study the influence of organic capping agent on the (electro)catalytic performances of NM nanocrystals.

In a typical experiment, 30 μL of 1M H_2PdCl_4 aqueous solution was added to 10 mL anhydrous DMF. The mixture was treated under 1 atm CO for 15 min, during which the orange solution turned light yellow. After the CO atmosphere was removed, 1 mL H_2O was added to the reaction mixture and within the first minute a dark blue color was clearly observed (Figure 1a). After 15 min, the product was separated and characterized. All operations were conducted at ambient temperature and no organic capping agent was used. As shown in Figure 1b, the brown–red $PdCl_4^{2-}$ precursor displayed UV/Vis absorption peaks at 336 nm and 436 nm, corresponding to d–d transition and ligand-to-metal charge transfer. In contrast, the yellow intermediate showed two discernible absorptions at 329 and 369 nm, indicating the

[*] Dr. H. Li, G. X. Chen, H. Y. Yang, X. L. Wang, J. H. Liang, P. X. Liu, M. Chen, Prof. N. F. Zheng
State Key Laboratory for Physical Chemistry of Solid Surfaces
Collaborative Innovation Center of Chemistry for Energy Materials and Department of Chemistry
College of Chemistry and Chemical Engineering
Xiamen University, Xiamen 361005 (China)
E-mail: nfzheng@xmu.edu.cn
Homepage: http://chem.xmu.edu.cn/person/nfzheng/index.html

[**] We thank the MOST of China (2011CB932403, 2009CB930703) and the NSFC (21131005, 21021061, 20925103, 20923004) for financial support. We also thank the XAFS station (BL14W1) of the Shanghai Synchrotron Radiation Facility (SSRF).

Supporting information for this article is available on the WWW under http://dx.doi.org/10.1002/anie.201303772.

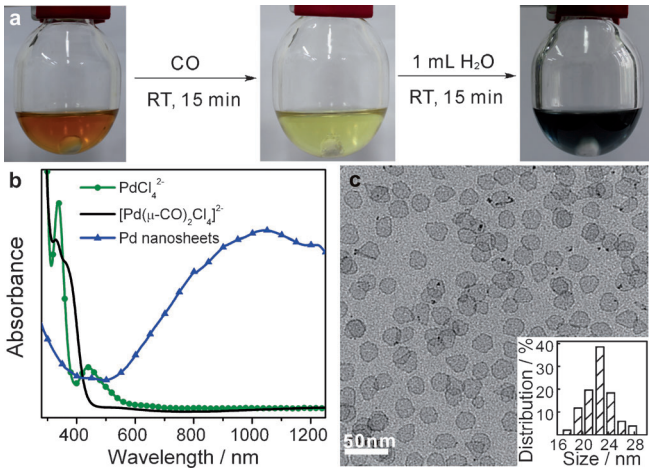

Figure 1. Photographs (a) and UV/Vis spectra (b) of $PdCl_4^{2-}$ in DMF, the yellow intermediate prepared by treating $PdCl_4^{2-}$ under CO, and the Pd nanosheets. c) TEM image of the Pd nanosheets. The inset shows the size distribution of Pd nanosheets.

change of the coordination environment of Pd. The dark blue solution formed after the addition of H_2O exhibited a broad and strong absorption particular in the near-infrared region, distinct from the absorptions of $PdCl_4^{2-}$ and the yellow Pd intermediate but similar to the absorption of our previously reported metallic Pd nanosheets.[21]

The transmission electron microscopy (TEM) image in Figure 1c shows that the blue solution indeed contained hexagonal Pd nanosheets which had an average diameter of 23 nm, the long diagonal of the hexagon. The high-resolution TEM (HRTEM) image of an individual Pd nanosheet shows the lattice fringes with interplanar spacing of 0.24 nm (Figure 2a), corresponding to 1/3(422) fringes of face-centered cubic (fcc) Pd.[21] The fcc structure of the metallic Pd nanosheets was also supported by their X-ray diffraction

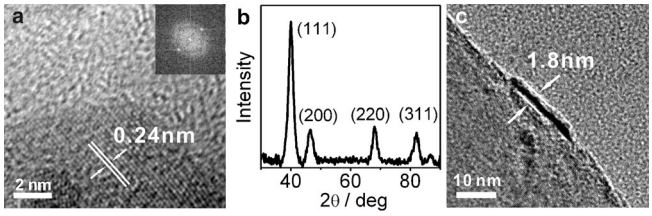

Figure 2. a) HRTEM image of a Pd nanosheet lying flat on the TEM grid. The inset is the corresponding Fourier transform pattern. b) XRD pattern of Pd nanosheets. c) TEM image of a single Pd nanosheet attached on a carbon nanotube.

(XRD) pattern (Figure 2b).The presence of 1/3(422) reflections suggests the presence of (111) stacking faults in the Pd nanosheets. These results are consistent with our previous observations on Pd nanosheets made from Pd^{II} acetylacetonate.[21] The upper and lower surfaces of the Pd nanosheets are Pd(111) facets while their side walls are Pd(100). Due to their ultrathin nature, the as-prepared Pd nanosheets tended to lie flat on the TEM grids, making it impossible to directly measure their thickness. To detect the thickness of the Pd nanosheets, carbon nanotubes (CNTs) were introduced to dispersions of the Pd nanosheets in DMF to allow the attachment of nanosheets on the outer surface of the nanotubes. As observed in Figure 2c, the Pd nanosheet has a thickness of 1.8 nm, which corresponds to less than ten atomic layers. According to our previous calculations using the discrete dipole approximation (DDA) method, the ultrathin nature is the main reason why Pd nanosheets have a well-defined surface plasmon resonance absorption feature.[21]

Ultrathin Pd nanosheets were nicely fabricated by simply mixing the solution of the yellow Pd intermediate with H_2O. This interesting phenomenon motivated us to gain a deeper understanding of the formation mechanism of the Pd nanosheets. Thus, we directed our efforts to resolving the structure of the yellow intermediate. As shown in Figure 3a, the FTIR spectrum of the yellow solution displays two bands at 1905 cm^{-1} and 1965 cm^{-1}. A signal at $\delta = 193.8$ ppm in ^{13}C NMR spectrum (Figure 3b) indicated the presence of a bridging ^{13}CO ligand in the yellow intermediate obtained by

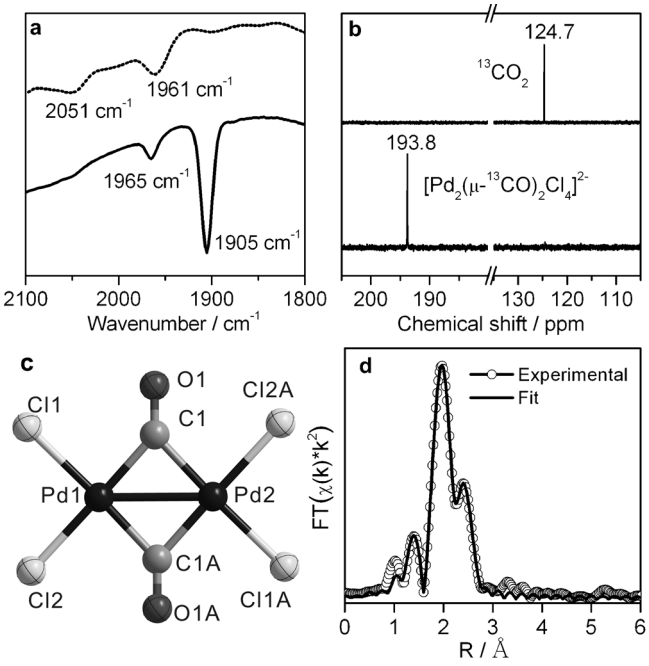

Figure 3. a) FTIR and b) ^{13}C NMR spectra of the solution of the yellow intermediate $[Pd_2(\mu\text{-}^{13}CO)_2Cl_4]^{2-}$ in DMF before (bottom) and after (top) addition of H_2O. c) The crystal structure of $[Pd_2(\mu\text{-}CO)_2Cl_4]^{2-}$ (counterion PPh_4^+ not shown). d) Curve fitting for the EXAFS spectrum of the yellow Pd intermediate.

using isotopically labeled ^{13}CO.[33] To determine its structure, we introduced tetraphenylphosphonium chloride (PPh_4Cl) to crystallize the yellow intermediate, and yellow crystals suitable for X-ray single crystal analysis were successfully obtained (see the Supporting Information (SI) for details). Single-crystal analysis indicated that the obtained yellow crystals contain $[Pd_2(\mu\text{-}CO)_2Cl_4]^{2-}$ clusters (Figure 3c and

Figure S1 (SI)) co-crystallized with PPh_4^+ in the triclinic space group $P\bar{1}$.[34] Each $[Pd_2(\mu\text{-}CO)_2Cl_4]^{2-}$ cluster has a Pd–Pd unit bridged by two CO ligands. The two Pd atoms have a separation of 2.6673(7) Å, indicating the presence of metal–metal bond. Besides two bridging CO ligands, each Pd is coordinated with two chloro ligands. Therefore, the Pd atoms in the $[Pd_2(\mu\text{-}CO)_2Cl_4]^{2-}$ cluster have an oxidation state of +1. The IR absorption bands at 1905 and 1965 cm^{-1} (Figure 3a and Figure S2 (SI)) are assigned to asymmetric and symmetric stretching modes of bridging CO ligands in $[Pd_2(\mu\text{-}CO)_2Cl_4]^{2-}$.[32,33]

Although a $[Pd_2(\mu\text{-}CO)_2Cl_4]^{2-}$ salt crystallizes, the yellow solution does not necessarily contain only this anion. To confirm that $[Pd_2(\mu\text{-}CO)_2Cl_4]^{2-}$ was the only product from the reaction of $PdCl_4^{2-}$ with CO, we conducted an X-ray absorption study on this intermediate solution under transmission mode at the Pd κ-edge (24.35 KeV). The Fourier transform of the κ2 weighted extended X-ray absorption fine structure (EXAFS) spectrum showed three dominant peaks at roughly 1.4, 2.0, and 2.4 Å, indicating three different coordination shells of the Pd atoms (Figure 3d). Bond information obtained from our single-crystal data was used to fit the EXAFS curve, and satisfying physical parameters from fitting were obtained (see the Supporting Information for details). The coordination numbers of Pd–Cl, Pd–C, and Pd–Pd from the fitting results are 2.2, 1.9, 0.9, respectively, close to the theoretical values (Table S1 (SI)). The bond lengths and Debye–Waller factors are all in reasonable ranges. The presence of only $[Pd_2(\mu\text{-}CO)_2Cl_4]^{2-}$ in the yellow intermediate indicates that CO can only reduce $PdCl_4^{2-}$ to Pd^I in DMF at room temperature.

Upon addition of H_2O at room temperature, $[Pd_2(\mu\text{-}CO)_2Cl_4]^{2-}$ was converted into uniform metallic Pd nanosheets. Our inductively coupled plasma mass spectrometry (ICP-MS) analysis on the product solution after removal of metallic Pd nanosheets suggested a nearly complete reduction of Pd^I to Pd^0. Moreover, the observations from the following two experiments indicated that free CO dissolved in DMF was not necessary for the formation of Pd nanosheets: 1) Although N_2 was bubbled through the yellow solution for 30 min to remove dissolved CO before introduction of H_2O, Pd nanosheets were still produced right after the addition of H_2O. 2) The addition of acidified H_2O to the DMF solution of single crystals of $(PPh_4)_2[Pd_2(\mu\text{-}CO)_2Cl_4]$ also led to the formation of a dark blue colloidal solution of Pd nanosheets. After the addition of H_2O to the DMF solution of $[Pd_2(\mu\text{-}{}^{13}CO)_2Cl_4]^{2-}$, as revealed in ^{13}C NMR spectrum (Figure 3b), a new ^{13}C peak at 124.7 ppm ascribed to $^{13}CO_2$ was detected, while the ^{13}C peak at 193.8 ppm corresponding to the bridging ^{13}CO ligands disappeared.[35] This result suggests that CO ligand in $[Pd_2(\mu\text{-}CO)_2Cl_4]^{2-}$ serves as the reductant to reduce Pd^I while it is oxidized to CO_2. The oxidation of one CO molecule to CO_2 provides two electrons to reduce both Pd^I sites in one $[Pd_2(\mu\text{-}CO)_2Cl_4]^{2-}$ unit to Pd^0. As a result, while all $[Pd_2(\mu\text{-}CO)_2Cl_4]^{2-}$ clusters in the DMF solution are converted into metallic Pd for the formation of Pd nanosheets, there is still enough CO to bind and protect the surface of the Pd nanosheets. The FTIR spectrum of the as-prepared Pd nanosheets (Figure 3a) shows two bands at 1961 and 2051 cm^{-1} associated with stretching modes of the bridging and linear-bonded CO on the Pd surface.[36] Taken together, after the addition of H_2O, one half of the bridging CO ligands on $[Pd_2(\mu\text{-}CO)_2Cl_4]^{2-}$ reduce Pd^I to Pd^0, and the other half help to protect Pd{111} and promote the formation of the ultrathin Pd nanosheets rather than irregular nanoparticles.

The most important feature of the Pd nanosheets prepared by the reaction of H_2O with $[Pd_2(\mu\text{-}CO)_2Cl_4]^{2-}$ is probably that their surface is free of any organic capping. To prove this, atomic force microscopy (AFM) was applied to measure the thickness of the Pd nanosheets obtained from $[Pd_2(\mu\text{-}CO)_2Cl_4]^{2-}$ (Figure 4a,b). An average thickness of 1.8 nm was observed from AFM. This thickness is the same as the result from TEM but significantly different from the value acquired from the PVP-capped Pd nanosheet (3.9 nm),[21] suggesting that the Pd nanosheets made from $[Pd_2(\mu\text{-}CO)_2Cl_4]^{2-}$ possess rather clean surfaces at least on their upper and lower sides.

To reveal the true properties of NM nanocrystals, many strategies like plasma cleaning,[37] oxidation–reduction,[38] and acid[39] and UV–ozone treatments[40] have been used to remove the capping agents on their surfaces. Hence, the high-surface-area Pd nanosheets free of organic capping we report here are desirable systems for evaluating the influence of organic capping agents on the catalytic performances of NM nanocrystals. The catalytic activity of the Pd nanosheets was assessed for the hydrogenation of styrene by supporting the nanosheets on carbon nanotubes (Pd/CNT) (see the

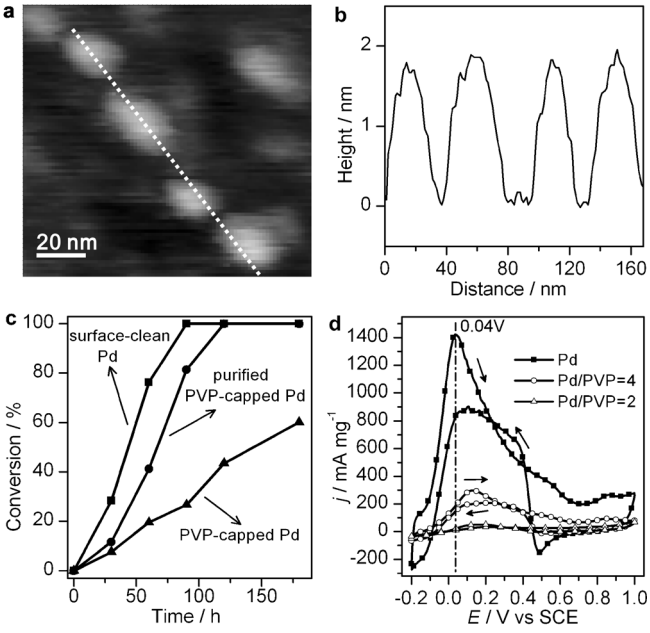

Figure 4. a) A representative AFM topographic image of the Pd nanosheets. b) Height profile along the dashed line in (a). c) Time profile of the conversion of styrene to ethylbenzene catalyzed by Pd nanosheets on CNT (squares), PVP-capped Pd nanosheets after purification (circles), PVP-capped Pd nanosheets (triangles). Styrene (8.66 mmol), 5 wt% Pd/CNT (5.6 mg), H_2 (1 atm), 25 °C, 15 mL ethanol. d) Cyclic voltammetry curve recorded in an aqueous solution containing 0.5 M H_2SO_4 and 0.25 M HCOOH at a scan rate of 50 $mV s^{-1}$ by using freshly made Pd nanosheets and in the presence of different amounts of PVP.

Supporting Information for details). For comparison, PVP-capped Pd nanosheets with an average diameter of 23 nm (same as that of Pd nanosheets reported here) were also synthesized by the previously reported procedure (TEM in Figure S3 (SI)). As shown in Figure 4c, Pd/CNT gave a conversion of 76.2% during the first hour under the given conditions, while the PVP-capped nanosheets gave only a 19.5% conversion at the same period. Since the two batches of Pd nanosheets have similar morphology, we ascribed this difference in activity to the partial blocking of active sites by PVP. Similar observations were made by other groups.[40] After careful cleaning using a mixed solvent of ethanol and acetone (see the Supporting Information for details), the purified PVP-capped Pd nanosheets exhibited an increase in catalytic activity, further indicating the negative effect of PVP blocking in catalysis. Recycling the Pd/CNT for seven times did not lead to a decrease in the catalytic activity (Figure S4 (SI)). After 10 cycles, the activity was only slightly decreased to 92%.

Compared with liquid-phase catalysis, electrocatalysis is even more sensitive to the surface cleanness of catalysts. For PVP-capped NM nanoparticles, tedious cleaning steps are typically required before they can serve as efficient catalysts. Being free of organic capping agent, the as-synthesized organic-free Pd nanosheets readily display excellent electrocatalytic performances in the oxidation of formic acid without any required pretreatment (see the Supporting Information for details). As shown in Figure 4d, the surface-clean Pd nanosheets gave a maximum current density of 1420 $mA\,mg^{-1}$ at the peak potential of 0.04 V, 0.1 V more negative than the value (0.14 V) acquired by PVP-capped Pd nanosheets.[21] This indicated that the surface-clean Pd nanosheets are better catalysts in HCOOH oxidation than the PVP-capped ones. And as expected, when the Pd nanosheets were mixed with PVP in PVP/Pd mass ratios of 1:4 and 1:2, the maximum current densities were obtained back at a higher potential (0.14 V) and decreased to 310 and 60 $mA\,mg^{-1}$, respectively. These results clearly suggest a deleterious effect of PVP on the (electro)catalysis of Pd nanocrystals and demonstrate the importance of developing synthetic methods to produce surface-clean Pd nanocatalysts.

In summary, we have demonstrated a facile synthetic method to prepare surface-clean uniform Pd nanosheets with a thickness of approximately 1.8 nm (only a few atomic layers thick) by simply mixing $[Pd_2(\mu\text{-}CO)_2Cl_4]^{2-}$ with H_2O. The $[Pd_2(\mu\text{-}CO)_2Cl_4]^{2-}$ complex was prepared by stirring a solution of $PdCl_4^{2-}$ in DMF solution under CO atmosphere and fully characterized by X-ray single-crystal analysis and X-ray absorption fine structure spectroscopy. Studies of the reaction mechanism suggest that the CO ligands in the complex serve as both reductant and capping agent for the formation of Pd nanosheets. The surface-clean Pd nanosheets produced by the developed method served as an excellent platform to evaluate the effect of organic capping on the catalysis and electrocatalysis of Pd nanocrystals.

Received: May 2, 2013
Published online: June 26, 2013

Keywords: electrocatalysis · hydrogenation · nanosheets · palladium

[1] T. K. Sau, A. L. Rogach, F. Jäckel, T. A. Klar, J. Feldmann, *Adv. Mater.* **2010**, *22*, 1805 – 1825.
[2] A. R. Tao, S. Habas, P. Yang, *Small* **2008**, *4*, 310 – 325.
[3] Y. Xia, Y. Xiong, B. Lim, S. E. Skrabalak, *Angew. Chem.* **2009**, *121*, 62 – 108; *Angew. Chem. Int. Ed.* **2009**, *48*, 60 – 103.
[4] C. Burda, X. Chen, R. Narayanan, M. A. El-Sayed, *Chem. Rev.* **2005**, *105*, 1025 – 1102.
[5] N. L. Rosi, C. A. Mirkin, *Chem. Rev.* **2005**, *105*, 1547.
[6] E. M. Larsson, C. Langhammer, I. Zorić, B. Kasemo, *Science* **2009**, *326*, 1091 – 1094.
[7] B. H. Wu, N. F. Zheng, *Nano Today* **2013**, *8*, 168 – 197.
[8] C. Wang, H. Daimon, T. Onodera, T. Koda, S. Sun, *Angew. Chem.* **2008**, *120*, 3644 – 3647; *Angew. Chem. Int. Ed.* **2008**, *47*, 3588 – 3591.
[9] H. Wang, H. Y. Jeong, M. Imura, L. Wang, L. Radhakrishnan, N. Fujita, T. Castle, O. Terasaki, Y. Yamauchi, *J. Am. Chem. Soc.* **2011**, *133*, 14526 – 14529.
[10] A. Callegari, D. Tonti, M. Chergui, *Nano Lett.* **2003**, *3*, 1565 – 1568.
[11] N. Tian, Z.-Y. Zhou, S.-G. Sun, Y. Ding, Z. L. Wang, *Science* **2007**, *316*, 732 – 735.
[12] F. Caruso, R. A. Caruso, H. Möhwald, *Science* **1998**, *282*, 1111 – 1114.
[13] M. Chen, B. H. Wu, J. Yang, N. F. Zheng, *Adv. Mater.* **2012**, *24*, 862 – 879.
[14] C. Y. Chiu, Y. J. Li, L. Y. Ruan, X. C. Ye, C. B. Murray, Y. Huang, *Nat. Chem.* **2011**, *3*, 393 – 399.
[15] B. T. Sneed, C.-H. Kuo, C. N. Brodsky, C.-K. Tsung, *J. Am. Chem. Soc.* **2012**, *134*, 18417 – 18426.
[16] L. Ruan, H. Ramezani-Dakhel, C. Y. Chiu, E. Zhu, Y. Li, H. Heinz, Y. Huang, *Nano Lett.* **2013**, *13*, 840 – 846.
[17] Y.-H. Chen, H.-H. Hung, M. H. Huang, *J. Am. Chem. Soc.* **2009**, *131*, 9114 – 9121.
[18] W. Niu, L. Zhang, G. Xu, *ACS Nano* **2010**, *4*, 1987 – 1996.
[19] B. Lim, M. J. Jiang, J. Tao, P. H. C. Camargo, Y. M. Zhu, Y. N. Xia, *Adv. Funct. Mater.* **2009**, *19*, 189 – 200.
[20] H. Ataee-Esfahani, Y. Nemoto, M. Imura, Y. Yamauchi, *Chem. Asian J.* **2012**, *7*, 876 – 880.
[21] X. Q. Huang, S. H. Tang, X. L. Mu, Y. Dai, G. X. Chen, Z. Y. Zhou, F. X. Ruan, Z. L. Yang, N. F. Zheng, *Nat. Nanotechnol.* **2011**, *6*, 28 – 32.
[22] X. Q. Huang, S. H. Tang, H. H. Zhang, Z. Y. Zhou, N. F. Zheng, *J. Am. Chem. Soc.* **2009**, *131*, 13916 – 13917.
[23] G. X. Chen, Y. M. Tan, B. H. Wu, G. Fu, N. F. Zheng, *Chem. Commun.* **2012**, *48*, 2758 – 2760.
[24] X. Q. Huang, Z. P. Zhao, J. M. Fan, Y. M. Tan, N. F. Zheng, *J. Am. Chem. Soc.* **2011**, *133*, 4718 – 4721.
[25] B. H. Wu, N. F. Zheng, G. Fu, *Chem. Commun.* **2011**, *47*, 1039 – 1041.
[26] Y. Dai, X. L. Mu, Y. M. Tan, K. Q. Lin, Z. L. Yang, N. F. Zheng, G. Fu, *J. Am. Chem. Soc.* **2012**, *134*, 7037 – 7080.
[27] X. Q. Huang, N. F. Zheng, *J. Am. Chem. Soc.* **2009**, *131*, 4602 – 4603.
[28] X. Q. Huang, H. H. Zhang, C. Y. Guo, Z. Y. Zhou, N. F. Zheng, *Angew. Chem.* **2009**, *121*, 4902 – 4906; *Angew. Chem. Int. Ed.* **2009**, *48*, 4808 – 4812.
[29] D. B. Dell'Amico, L. Labella, F. Marchetti, S. Samaritani, *Coord. Chem. Rev.* **2010**, *254*, 635 – 645.
[30] Q. Xu, *Coord. Chem. Rev.* **2002**, *231*, 83 – 108.
[31] A. D. Gel'man, E. Meilakh, *Dokl. Akad. Nauk SSSR* **1942**, *36*, 171 – 188.
[32] P. L. Goggin, R. J. Goodfellow, I. R. Herbert, A. G. Orpen, *J. Chem. Soc. Chem. Commun.* **1981**, 1077 – 1079.

[33] S. Baig, B. Richard, P. Serp, C. Mijoule, K. Hussein, N. Guihéry, J.-C. Barthelat, P. Kalck, *Inorg. Chem.* **2006**, *45*, 1935 – 1944.
[34] Crystallographic data for $(Ph_4P)_2[Pd_2(\mu\text{-}CO)_2Cl_4]$: yellow block crystal, $a = 9.4793(17)$ Å, $b = 10.2608$ (18) Å, $c = 13.208(2)$ Å, $V = 1120.5$ (3) Å^3, $Z = 2$, $Mo_{K\alpha}$, $T = 293$ K, $2\theta = 56.94°$. 6923 reflections were measured, of which 5001 were unique with $R_{int} = 0.1218$. Final $R_1 = 5.72\,\%$, $wR_2 = 0.1470$ for 271 parameters and 4771 reflections with $I > 2\sigma(I)$. See Tables S2 and S3 in the Supporting Information for details.
[35] G. R. Fulmer, A. J. Miller, N. H. Sherden, H. E. Gottlieb, A. Nudelman, B. M. Stoltz, J. E. Bercaw, K. I. Goldberg, *Organometallics* **2010**, *29*, 2176 – 2179.
[36] S. Carrez, B. Dragnea, W. Q. Zheng, H. Dubost, B. Bourguignon, *Surf. Sci.* **1999**, *440*, 151 – 162.
[37] B. Gehl, A. Frömsdorf, V. Aleksandrovic, T. Schmidt, A. Pretorius, J. I. Flege, S. Bernstorff, A. Rosenauer, J. Falta, H. Weller, *Adv. Funct. Mater.* **2008**, *18*, 2398 – 2410.
[38] I. Lee, R. Morales, M. A. Albiter, F. Zaera, *Proc. Natl. Acad. Sci. USA* **2008**, *105*, 15241 – 15246.
[39] V. Mazumder, S. Sun, *J. Am. Chem. Soc.* **2009**, *131*, 4588.
[40] M. Crespo-Quesada, J.-M. Andanson, A. Yarulin, B. Lim, Y. Xia, L. Kiwi-Minsker, *Langmuir* **2011**, *27*, 7909 – 7916.

